



Wavelength-independent ultrafast dynamics and coherent oscillation of a metal–carbon stretch vibration in photodissociation of $\text{Cr}(\text{CO})_6$ in the region of 270–345 nm

S.A. Trushin, K. Kosma, W. Fuß *, W.E. Schmid

Max-Planck-Institut für Quantenoptik, D-85740 Garching, Germany

Received 29 June 2007; accepted 25 September 2007

Abstract

In the group-6 metal hexacarbonyls a number of metal-to-ligand charge-transfer (MLCT) and ligand-field (LF or $d \rightarrow d$) states can be excited in the near UV. The latter are repulsive. In equilibrium geometry, most of them are higher than the MLCT states. We probed the dynamics of photodissociation of $\text{M}(\text{CO})_6 \rightarrow \text{M}(\text{CO})_5 + \text{CO}$ ($\text{M} = \text{Cr}$; some data also for $\text{M} = \text{Mo}$) with improved time resolution (10–40 fs), pumping at different wavelengths (mainly 270–345 nm) and probing by nonresonant photoionization. The initial relaxation (e.g. within 12.5 fs from T_{1u} excited at 270 nm) is assigned to direct crossing over to the repulsive surface, from where the subsequent dissociation is also remarkably fast (18 fs in this example). That is, there is no detour via the lowest excited singlet state, in contrast to the usual assumption. Also with 318 and 345 nm excitation a direct $\text{MLCT} \rightarrow \text{LF}$ relaxation seems to occur before dissociation. The product $\text{M}(\text{CO})_5$ is generated in the S_1 state, also at pump wavelengths (345 nm) with barely sufficient energy. It relaxes to S_0 through a Jahn–Teller induced conical intersection along pseudorotation coordinates, which stimulates a coherent oscillation in S_0 in this vibration. A higher-frequency oscillation, assigned to totally symmetric MC stretch vibrations, is already found in the Franck–Condon region; it persists (with different wavenumbers) also during dissociation and over the subsequent product states. This vibration is transverse to the valley of dissociation, which is barrierless. The wavelength-independent mechanism also implies that there is no triplet contribution (which was previously supposed at long wavelengths) to photochemical dissociation of the hexacarbonyls.
© 2007 Elsevier B.V. All rights reserved.

Keywords: Conical intersections; Coherent oscillations; Femtochemistry; Jahn–Teller effect; Kasha rule; Potential energy surfaces; Pseudorotation

1. Introduction

UV photolysis eliminates a CO group from metal carbonyls $\text{M}(\text{CO})_n$ [1,2], leaving unsaturated metal carbonyls $\text{M}(\text{CO})_{n-1}$ behind which are prototypes of unsaturated complexes that are often used in processes such as CH activation [3]. Quite a number of states are energetically in reach for UV wavelengths: The ligand-field (LF or $d \rightarrow d$) excited group involves lifting of a π -bonding d electron to a σ -antibonding d orbital, resulting in a number of repulsive states of different symmetries. The group of

metal-to-ligand charge transfer (MLCT) states are formed by promoting a metal d electron to one of the CO π^* orbitals. They are not expected a priori to be dissociative, because they correlate with an ion pair that is subjected to Coulomb attraction. The MLCT states of suitable symmetry (T_{1u} for an octahedral molecule) are connected by high transition moments with the ground state, whereas the LF transitions are symmetry forbidden and correspondingly weak. Since the work of the Baerends [4–6] and Pierloot [7] groups it is known that the MLCT states lie below most of the LF states in the group-6 carbonyls $\text{M}(\text{CO})_6$. This is also confirmed in a recent publication of the Daniel group on $\text{Cr}(\text{CO})_6$ [8]. The lower of the two T_{1u} states is populated by optical excitation near 278 nm (36000 cm^{-1}) in this molecule and near 287 nm in

* Corresponding author. Fax: +49 89 32905 200.
E-mail address: w.fuss@mpq.mpg.de (W. Fuß).

Mo(CO)₆ and W(CO)₆. The corresponding absorption bands are broad (halfwidth $\approx 4000\text{ cm}^{-1}$) [9,10]. The calculations [4,5] found furthermore that from one of the lowest MLCT states (T_{2u}) the population can flow via an avoided crossing to an LF surface, which steeply declines from higher energy down to the dissociation product; but the other MLCT states rise along the M–C stretch coordinate and thus seem not dissociative [4,5].

In femtosecond experiments with 267 nm excitation and probing by nonresonant (800 nm) photoionization of M(CO)₆ (M = Cr, Mo, W) [11,12], Fe(CO)₅ [13], Ni(CO)₄ [14] and other carbonyls [15] we found previously that the molecules indeed do not directly dissociate from the T_{1u} (or analogous) state but change the electronic state before. We pointed out that Jahn–Teller active coordinates play an important role for the initial relaxation. We also found that M(CO)_{*n*–1} is initially produced in its first excited singlet state S_1 ; from there, many of the unsaturated carbonyls relax along a pseudorotation coordinate to S_0 (which explains the isomers observed in photosubstitution reactions [12,16–18]), where sometimes coherent oscillations can be observed; one of them, Ni(CO)₃, luminesces instead [14]. On initial singlet excitation, any triplet channel (considered as a possibility in textbooks [2,19]) was excluded for all the ultrafast processes; this was, for instance, inferred from the increase of all lifetimes in the series M = Cr, Mo, W, which is the opposite of the trend expected, if intersystem crossing were involved. The production of singlet Fe(CO)₄ (instead of the previously assumed triplet that is the ground state of this unsaturated carbonyl) from Fe(CO)₅ has been confirmed by time-resolved electron diffraction [20] and the mechanism assessed in view of previous findings [21]. The dynamics of dissociating Cr(CO)₆ and in particular the pathway after formation of Cr(CO)₅ has been confirmed by trajectory [22] and wave packet dynamics [23] calculations on CASSCF surfaces.

The theory [4–6] suggests one relaxation step in the intact Cr(CO)₆ from the T_{2u} -MLCT state to a dissociative LF state. On exciting the higher-lying T_{1u} state in our previous work we found two time constants before the dissociation process [11,12] (see also the survey including other carbonyls in [15]). We suggested that the molecule first relaxes from the initial T_{1u} MLCT state via a Jahn–Teller induced conical intersection to the lowest (or nearly lowest [4–6,8]) MLCT state (T_{2u}) and only then to the dissociative surface. In the present work we find with 5–15 times improved time resolution that the process with the putative second time constant is actually a highly overdamped Cr–C stretch oscillation, taking place during dissociation. Analogous results are found for Mo(CO)₆. The same oscillation is also found – with different frequencies – in the subsequent observation windows, the S_1 and S_0 states of the dissociation product Cr(CO)₅. Whereas the very first time constant in Cr(CO)₆ is even shorter than previously found, the other time constants (those that are ≥ 25 fs, including also all of Mo(CO)₆) are confirmed, as is also the pseudorotation vibration in Cr(CO)₅.

The idea [4,12] that the first step after T_{1u} excitation (at 270 nm) represents relaxation down to T_{2u} , one of the lowest excited singlet states, is consistent with the Kasha rule. To check it, we investigated the dynamics of Cr(CO)₆ also at longer wavelengths (318 and 345 nm), where the T_{2u} state can be directly excited. The results are better consistent with a direct MLCT \rightarrow LF relaxation instead of an initial downward step. The first time constant is also reported for some more wavelengths.

2. Experimental

The experiments were performed in an improved version of our previous setup [11,12], primarily using 5–15 times shorter pulses. Briefly, M(CO)₆ was excited in the gas phase (pressure 10^{-4} to 10^{-7} mbar, background 10^{-9} mbar) by weak femtosecond UV pulses (10^9 W cm^{-2} , $25\text{ }\mu\text{J cm}^{-2}$, typically ≈ 30 fs, in some measurements 10 fs), tuned in the range 270–345 nm, and then after variable delay probed by nonresonant ionization (10^{13} W cm^{-2} , 810 nm, ≈ 10 –20 fs); the signals are the yields of the parent and fragment ions M(CO)_{*n*}⁺ determined in a time-of-flight mass spectrometer as functions of the delay time. The time zero was taken from the maximum of the Xe⁺ signal from Xe added in all measurements. For M = Cr we measured all the ions ($n = 6, \dots, 0$), for M = Mo only M(CO)₆⁺ and M(CO)₅⁺.

The generation of the 10–17 fs 810-nm pulses is reported in [24,25], that of the tunable 30-fs UV pulses in [25], and that of the 10-fs UV pulses will be reported later in detail. Briefly, we shortened the pulses (810 nm, 45 fs, 1 kHz) of a commercial Ti-sapphire laser system, by focusing ($f = 2$ m) 1 mJ of them into a cell (length 1.5 m, equipped with quartz-glass windows of 0.2 mm thickness) filled with 200 mbar Ar + 800 mbar He (instead of atmospheric-pressure of Ar as in [24]). Under these conditions the pulses are self-phase modulated and acquire a chirp, which can be used to compress the pulses to 17 fs (determined by a commercial autocorrelator) by reflection from chirped mirrors [24,25]. Using 1 bar of Ar instead of the gas mix gives rise to a pulse duration of 10 fs [24]. Part ($\approx 10\text{ }\mu\text{J}$) of this radiation (10–17 fs) is used for probing.

Another part (0.8 mJ) served for generation of the UV (pump) wavelengths by two different methods: (1) frequency tripling in a short argon cell and (2) supercontinuum generation in a long Ar cell.

- (1) For the third harmonic, the radiation was refocused into a second Ar cell (18 mm length), that has pinholes (0.7 mm diameter) for entrance and exit of the radiation. This cell was embedded in a larger cell, where a pump maintained a pressure of about 5 mbar of Ar, whereas in the 18-mm cell the pressure of the flowing Ar was ≈ 200 mbar. The emerging radiation contained 800 nJ of the third harmonic (270 nm), corresponding to 0.1% of conversion efficiency. Its bandwidth was 9 nm. It was isolated by reflection from a

dichroic mirror. Before using it as a pump pulse in the experiment, it was shortened by a prism compressor (pair of CaF₂ prisms and a plane mirror) to 28 fs [25]. This was necessary, because after generation the UV pulses traveled through 2.5 m of air and a 0.5-mm CaF₂ window, so that the pulses were lengthened by the corresponding dispersion. This was even worse, if we started from pulses of 10 fs instead of 17 fs, which are spectrally broader than the longer pulses. In a more recent setup, we therefore put the beam path after UV generation completely into vacuum (details to be reported later). In this case we used shorter (10–12 fs) IR pulses and got UV pulses slightly below 10 fs [26]. Some of the time-resolved data are from this vacuum setup.

- (2) For generating the supercontinuum, the 810-nm 10-fs radiation is limited by a diaphragm in diameter (to 4 mm) and energy (to 0.4 mJ) and refocused ($f = 1$ m) into a cell with atmospheric-pressure Ar. The UV radiation of the desired wavelength (in particular 318 nm) was again isolated by reflection from dielectric mirrors. In the setup with beam path in air, compression by the prisms resulted in a pulse duration of 30 fs. In the more recent setup with the vacuum beam path, we obtained 9.7 fs at 282 nm [26].

The weak absorption (2×10^{-18} cm²) of Cr(CO)₆ at 345 nm required a stronger pump pulse. We used the radiation generated in the commercial (TOPAS, Light Conversion) optical parametric generator combined with various nonlinear frequency conversion steps, as previously (e.g. [27]). It delivered pulses of a few μ J with durations of 42 fs after a prism compressor.

The UV pulse durations were determined by ionizing xenon in the pump–probe experiment: The Xe⁺ signal represents the cross correlation function between the pump intensity and the fifth–sixth power (depending on the UV photon energy) of the probe intensity. The durations of the 810-nm pulses were measured by a commercial autocorrelator.

As mentioned, the other part (≈ 10 μ J) of the radiation, taken aside before UV generation, was used for probing. The probe delay was varied in steps of 3.3 fs (0.5 μ m). Both beams were combined before the ionization setup by a mirror with a hole. Pump and probe pulses are focused by mirrors (focal lengths 1 and 0.7 m, respectively) into the ionization region of the mass spectrometer.

3. Results

3.1. Cr(CO)₆

The gas-phase UV spectrum of Cr(CO)₆ measured with saturated vapor in 1- and 10-cm cells is shown in Fig. 1. Taking the absorption cross section (5×10^{-17} cm²) at the first T_{1u} maximum (278–280 nm) from the value in acetonitrile solution [9,28], the vapor pressure can be calculated to be 0.15 mbar (literature value 0.35 mbar at 20 °C [29]). The

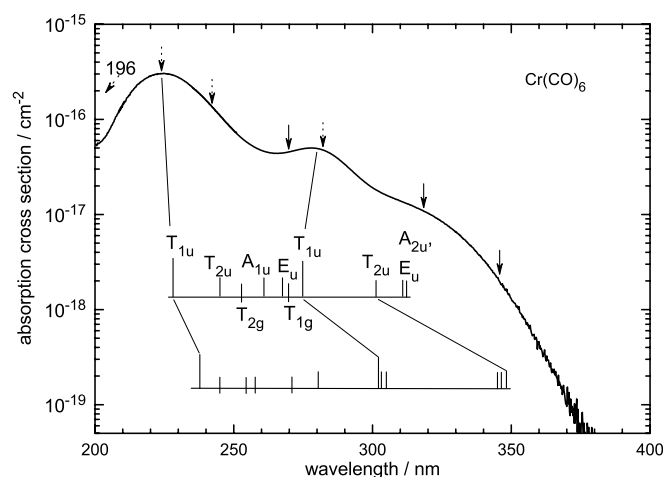


Fig. 1. Gas-phase UV spectrum of Cr(CO)₆. The absorption cross section at the 278-nm maximum was set equal to the value [9] in acetonitrile solution at 280 nm. The calculated positions of states are also given in the upper [8] and lower [7] ladders; longer lines indicate allowed transitions (T_{1u}), the lines for MLCT (u symmetry) and LF states (g symmetry) ending on and below the horizontal line, respectively. The arrows indicate the employed excitation wavelengths (dotted, where only τ_1 was investigated).

figure also indicates the pump wavelengths and the location of the states of the MLCT (u symmetry) and LF (g symmetry) groups, as predicted by two CASPT2 calculations [7,8]. The wavelengths 270 and 282 nm are in the wings of the longer-wavelength T_{1u} band, whereas 318 and 345 nm excite the precursor bands [28], whose nature (symmetry-forbidden MLCT band or triplet transitions) are still under discussion in the literature [4–8,28] (see Sections 1 and 5). The second allowed transition is excited at 224 nm, and 242 nm is in the wing of it; a satellite of it is excited at 196 nm [30]. Excitation at 162 nm (7.65 eV) is just below the ionization limit (8.14 eV [31]), so that probably a Rydberg state is populated. With these four wavelengths and with 282 nm, we only determined the very first time constant.

The ion signals Cr(CO)_n⁺, $n = 6, \dots, 0$, are generated from different locations L_i on the potential energy surfaces (PES). This is schematically indicated in Fig. 2 (see also [11]). The L_i are consecutively populated and differ in their mass spectra (upper part of Fig. 2). The L_i populations are modeled by rate equations. Their solution results in sums of temporal exponentials (lifetimes τ_i of the L_i). The signals themselves are linear combinations of such (sums of) exponentials, convoluted with the instrumental function (correlation of the pump pulse with a suitable power p of the probe pulse; p is usually the number of probe photons required to ionize L_i , but can be smaller in the case that there is an intermediate resonance that is saturated. Therefore we treat p as a parameter in the fit procedure if necessary). A fit of such functions to the signals yields the time constants τ_i and the relative probabilities ${}^n\sigma_i$ to generate the ion Cr(CO)_n⁺ from location L_i . Such a fit is carried out as a first step, in which oscillations can be ignored,

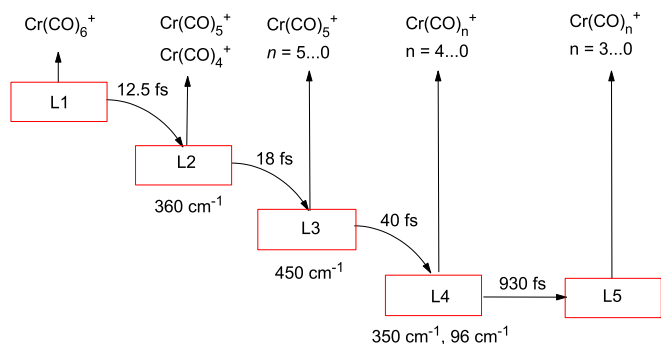


Fig. 2. Scheme of the consecutive locations L_i and their lifetimes τ_i on the potential surfaces in the dynamics of $\text{Cr}(\text{CO})_6$ dissociation. Wavenumbers are also given for oscillations observed in L_i . Mass spectra (fragmentation patterns) obtained from each L_i are schematically indicated above the vertical arrows; quantitative fragment intensities are represented by ${}^n\sigma_i$, for which values are given in the tables. The values for τ_i given in the scheme are for a pump wavelength of 270 nm. The same scheme (with different values for τ_i) is used for all pump wavelengths.

since the nonperiodic fit function averages over them. It is practical to first extract the later time constants, outside the pump–probe overlapping region, where convolution is not necessary; these constants are then fixed in the next step, a full fit beginning from the earliest times, with convolution.

3.1.1. Dynamics of $\text{Cr}(\text{CO})_6$ excited at 270 nm

These wavelengths populate the same state (T_{1u}) as in our previous work [11,12]. Figs. 3–6 show the measured ion yields for $\text{Cr}(\text{CO})_n^+$ with $n = 6, \dots, 3$ together with simulation curves, and Table 1 lists the time constants τ_i and ionization cross sections ${}^n\sigma_i$ evaluated from these data. The smaller fragments were only incompletely evaluated (no iterative improvement of the simulation parameters), because the time constants and oscillation frequencies agreed with those of the other signals and/or those of our previous work. As said above, we first determined the longer time constants. They agree with the previous values [11,12] ($\tau_4 = 930$ fs and $\tau_5 = \infty$, i.e. >500 ps, both from $\text{Cr}(\text{CO})_n^+$ with $n = 3, \dots, 0$, not shown in this long-time range, although a trace of the τ_4 process can be seen in the inset of Fig. 5. We did not look for the small-amplitude component with lifetime 39 ps found previously at 267 nm and assigned to further dissociation of $\text{Cr}(\text{CO})_4$ in [12]). $\tau_3 = 40$ fs was determined by single exponential fitting to $\text{Cr}(\text{CO})_5^+$ and $\text{Cr}(\text{CO})_4^+$ in the range of ca. 120–230 fs (Figs. 4a and 5); this value was later confirmed by a fit over the full time range, including the other time constants and the oscillations. Since L_4 does not contribute to the $\text{Cr}(\text{CO})_5^+$ signal (and nearly not to $\text{Cr}(\text{CO})_4^+$) (Table 1), it was not necessary to take τ_4 into account for its evaluation. Note that $\text{Cr}(\text{CO})_4^+$ signal shows a strong oscillatory modulation at later times (discussed below). With τ_3 fixed, $\tau_2 = 18$ fs was then determined from $\text{Cr}(\text{CO})_5^+$ by doubly exponential fitting for times ≥ 60 fs (Fig. 4a inset). The preceding $\tau_1 = 12.5$ fs could be determined by singly exponential fitting (with convolution in the full fit, or without in the

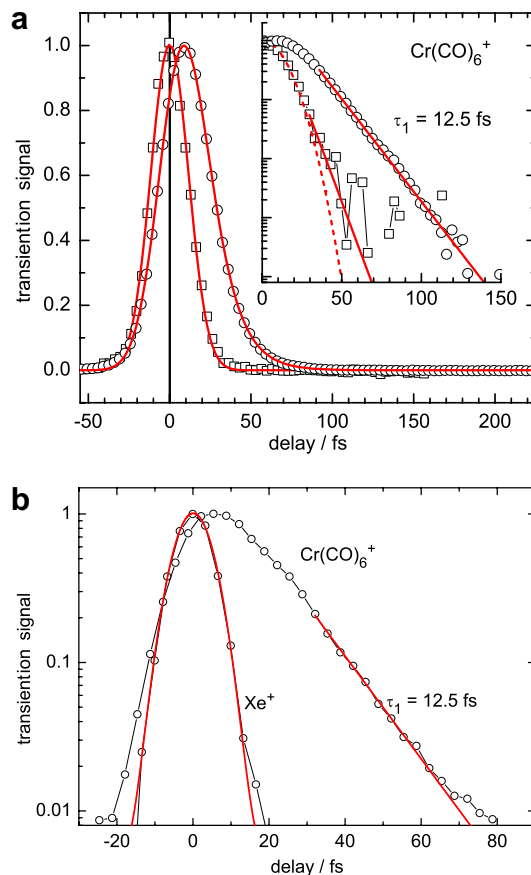


Fig. 3. Measured ion yields of $\text{Cr}(\text{CO})_6^+$ using the pump pulses of 270 nm and pulse duration (a) 30 fs and (b) 10 fs, together with simulation curves. The Xe^+ data represent the cross correlation of the pump with the fifth power of the probe, indicating the instrumental function.

range 40–110 fs outside the pump–probe overlapping region) from the $\text{Cr}(\text{CO})_6^+$ signal (Fig. 3a inset), which is only produced from L_1 and from nowhere else (Table 1). The same τ_1 was also found from the parent ion with the shorter (10 fs) pump pulses at 270 nm (Fig. 3b). The longer time constants were not checked with these shorter pulses. (It may be remarkable that the kinetic description works so well not only in the exponential decay of Fig. 3b but also at very short times, near the signal maximum in Fig. 3a and b. This is not self-evident, because coherent effects or some consequences of the acceleration phase of the wave packet might have been expected at such short times. On the other hand, it is not so surprising: The width of the molecular absorption is larger than the coherent width of the 10-fs pulses: >4000 cm^{-1} as compared to 1470 cm^{-1} . However, some deviations from the kinetic description do occur at later times, in the form of the observed coherent oscillations.)

At this step, the set of time constants was used to check whether all signals can be reproduced by them over the full time range, either to improve their values or to detect from deviations any further process. An obvious deviation is the oscillation in the decaying part ($\tau_4 = 40$ fs) of the

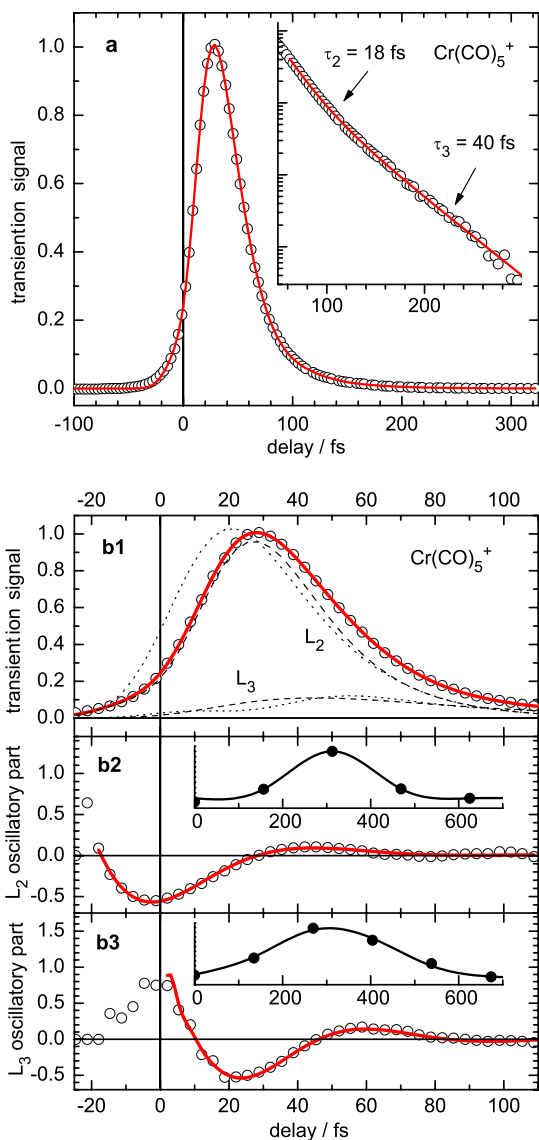


Fig. 4. Ion yields of $\text{Cr}(\text{CO})_5^+$ with 270-nm 30-fs pump, together with simulation curves. In the inset of (a) one can recognize the exponential parts, in (b1) how they can be simulated by contributions (thin lines) from L_2 and L_3 ; the dotted thin lines only contain the exponential parts, the broken lines also the oscillations. The latter are isolated (function f_{osc} of Eqs. (1) and (2)) in (b2) and (b3), with the insets showing the Fourier transforms of them (abscissa unit: cm^{-1}).

$\text{Cr}(\text{CO})_4^+$ signal, and a closer inspection reveals more such modulations.

Signal oscillations are interpreted as a molecular vibration in L_i , which modulates the ionization probability ${}^n\sigma_i$ by a periodic function f_{osc} (period τ_{osc} , amplitude A , phase delay φ) which itself also contains a decay term (dephasing time τ_{deph}):

$${}^n\sigma_i = {}^n\sigma_i^0(1 + f_{\text{osc}}) \quad (1)$$

$$f_{\text{osc}} = A \exp(-t/\tau_{\text{deph}}) \cos(2\pi t/\tau_{\text{osc}} - \varphi) \quad (2)$$

Where two different oscillations are active, we add another periodic factor $(1 + f_{\text{osc}2})$ in (1) with corresponding

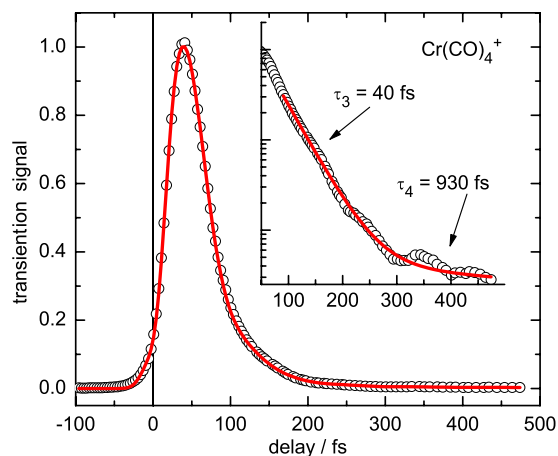


Fig. 5. Ion yields of $\text{Cr}(\text{CO})_4^+$ with 270-nm 30-fs pump. In the inset the simulation curves contain only the exponential parts.

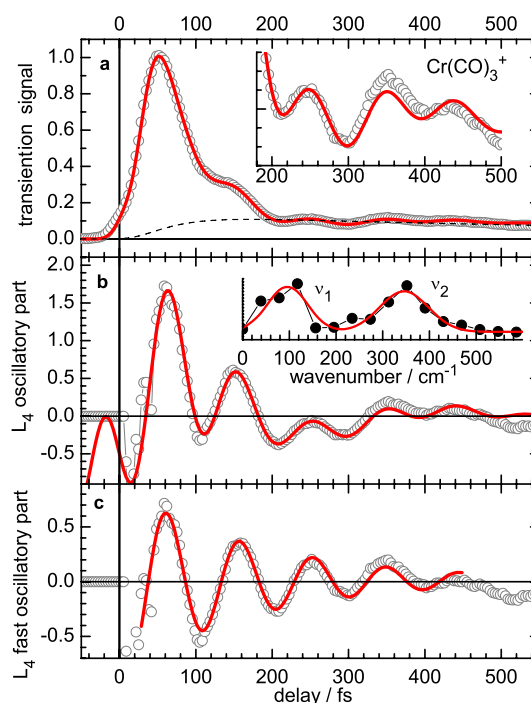


Fig. 6. Ion yields of $\text{Cr}(\text{CO})_3^+$ with 270-nm 30-fs pump. In (a) the broken line indicates the contribution from L_4 ; the later part of the signal is magnified in the inset. (b) shows the periodic part of the signal from L_4 (two f_{osc} evaluated with Eqs. (1) and (2)), with the Fourier transform in the inset. Subtracting from (b) the slow oscillation (which persists to >1 ps) reveals more clearly the fast oscillation (c).

parameters in (2). To extract the parameters, it is easiest to begin with a signal in a time range, where practically only one location contributes. An example is $\text{Cr}(\text{CO})_4^+$ in the range 120–230 fs, where L_2 has already decayed ($\tau_2 = 18$ fs); L_4 does nearly not contribute to this signal in this time range, because ${}^4\sigma_4$ is small (0.002, Table 1). This part of the signal is then divided by the decaying L_3 population, the result being $\propto(1 + f_{\text{osc}})$. The function f_{osc} is then Fourier transformed, to obtain the period τ_{osc} (73 fs, corresponding to a wavenumber of 465 cm^{-1}). This

Table 1
Pump laser at 270 nm: life times τ_i and effective ionization–dissociation cross sections ${}^n\sigma_i$

L_i	L_1	L_2	L_3	L_4	L_5
τ_i/fs	12.5 ± 0.5	18 ± 2	40 ± 3	930 ± 100	∞
$\text{Cr}(\text{CO})_6^+$	1	0	0	0	0
$\text{Cr}(\text{CO})_5^+$	0	1.0	0.082	0	0
$\text{Cr}(\text{CO})_4^+$	0	1.0	0.440	0.002	0
$\text{Cr}(\text{CO})_3^+$	0	0	1.0	0.063	0.013

In locations L_2 – L_4 , periodic modulations (Eqs. (1) and (2)) of ${}^n\sigma_i$ were also used. The data for $\text{Cr}(\text{CO})_n^+$ with $n = 2, \dots, 0$ were not evaluated in detail. Error limits are standard deviations for the values determined in ≥ 8 different scans.

time in turn is inserted in the function (2), which is then remultiplied by the time-dependent L_3 population and then used to simulate this part of the $\text{Cr}(\text{CO})_4^+$ signal; in this way one obtains τ_{deph} and φ (Table 3), and the quality of the fit can be judged. Since L_3 also contributes to $\text{Cr}(\text{CO})_5^+$, the same modulation (with the same τ_{osc} and τ_{deph} , but possibly different A and φ) is also expected in this signal. The $\text{Cr}(\text{CO})_5^+$ is therefore simulated by the exponential L_2 and L_3 populations (with the τ_i and ${}^4\sigma_i$ determined above), each multiplied by the periodic functions (1), in which τ_{osc} for L_3 is fixed. (The modulated L_3 contribution is shown in the lowest panel of Fig. 4b.) This results also in a value for τ_{osc} (93 fs, 362 cm^{-1}) for L_2 (middle panel of Fig. 4b). Because of the short τ_1 (12.5 fs), one cannot expect to detect such an oscillation also in L_1 (see, however, the results at longer wavelengths and those of the heavier carbonyl).

Much more prominent oscillations are observed from L_4 . This is illustrated in Fig. 6 with the $\text{Cr}(\text{CO})_3^+$ signal. Subtracting the L_3 contribution from the total signal (upper panel) and dividing by the L_4 population (broken line) results in the periodic modulation (f_{osc} shown in the middle panel, with the Fourier transform as inset); after subtracting the slowly oscillating part (350 fs, 95 cm^{-1}), the fast oscillation (95 fs, 350 cm^{-1}) is clearly revealed in the lower panel. (As explained after Eq. (2), we used two factors ($1 + f_{\text{osc}}$) as in Eq. (1) for evaluation of the L_4 signals.)

The slow oscillation agrees with our previous findings, whereas the fast oscillations are only now detected with the better time resolution.

3.1.2. Initial dynamics of $\text{Cr}(\text{CO})_6$ excited at 318 and 345 nm

Whereas 270 nm is near the maximum of the T_{1u} absorption, the two longer wavelengths coincide with two weaker bands, which according to Beach and Gray [9] can be discerned in the long-wavelength wing of the gas-phase spectrum (Fig. 1).

The time-resolved measurements and evaluations at both wavelengths were done in the same way as at 270 nm. The signals $\text{Cr}(\text{CO})_n^+$ with $n = 6, \dots, 4$ were analysed in detail. Measured data are given in the Supplementary data. Also the ${}^n\sigma_i$ are listed there. Here we only

Table 2
Time constants τ_i found for $\text{Cr}(\text{CO})_6$ with different pump wavelengths λ_{pump}

λ_{pump} (nm)	τ_1/fs	τ_2/fs	τ_3/fs	τ_4/fs
270	12.5 ± 0.5	18 ± 2	40 ± 3	930 ± 100
318	19 ± 1	20 ± 2	35 ± 3	1200 ± 100
345	21 ± 1	22 ± 2	25 ± 3	1500 ± 100

Error limits are standard deviations for the values determined in ≥ 8 different scans.

summarize the time constants (Table 2) and the data for the oscillations found (Table 3), comparing them also with the corresponding values for 270-nm excitation. At all wavelengths, the signals can be simulated by the same number of time constants; their values varying by less than a factor of 2. Also the number of oscillations is the same. It is worth noting, however, that in contrast to 270 nm, with the longer wavelengths an oscillation was also found in the parent ion and hence in L_1 (Table 3). It might well be that the difference is only due to the nearly twice longer lifetimes τ_1 at 318 and 345 nm, that provide a chance to detect a periodic modulation (note that $\tau_{\text{osc}} > \tau_1$).

In a first variant of the evaluation, τ_{osc} in L_2 – L_4 was fixed to the values found with 270 nm. The idea was that these locations on the PES represent electronic states of $\text{Cr}(\text{CO})_5$, that are reached in all three cases (see Section 4). However, vibrational frequencies can (slightly) depend on the available excess energy, for example due to anharmonicity. Therefore we also allowed the fit procedure to vary τ_{osc} in L_2 – L_4 . In fact, the quality of the simulation improves a little with oscillation frequencies that are lower by about 10% at 318 than at 270 nm. Because this variation is near the error limit of the fixed values, Table 3 lists only the latter.

3.2. Initial dynamics of $\text{Cr}(\text{CO})_6$ excited at 290, 242, 224, 196 and 162 nm

In experiments with different organic molecules we often add $\text{Cr}(\text{CO})_6$ (instead of Xe) for preliminary alignment of pump and probe both in space and time: The long-lived fragment-ion signals permit to find the overlap also, if one is still far off, whereas the short-lived parent-ion signal allows to find the time zero and determine the instrumental function. Thus we can report on τ_1 with pump wavelengths such as 224 nm [27] (exciting the second T_{1u} state) or 242 nm (in the wing of this band) [27], 196 nm [32] (pumping a weaker spectral satellite; see the spectrum in [30]) or 162 nm (fifth harmonic of the fundamental, exciting probably a Rydberg state of $\text{Cr}(\text{CO})_6$). With these shorter pump wavelengths the lifetimes – listed in Table 2a – are longer. This table also gives the value ($\tau_1 = 14$ fs) at 282 nm, determined in [26] with pulses from the supercontinuum.

3.3. Dynamics of $\text{Mo}(\text{CO})_6$ excited at 270 nm

The carbonyl of molybdenum was only briefly investigated, exciting it at 270 nm, in the wing of the T_{1u} band

Table 2a

First time constants τ_1 found in $M(\text{CO})_6$ (from the $M(\text{CO})_6^+$ signal) with different pump wavelengths

	$\text{Cr}(\text{CO})_6$	$\text{Cr}(\text{CO})_6$	$\text{Cr}(\text{CO})_6$	$\text{Cr}(\text{CO})_6$	$\text{Cr}(\text{CO})_6$	$\text{Mo}(\text{CO})_6$
$\lambda_{\text{pump}}/\text{nm}$	282	242 [27]	224 [27]	196	162	270
τ_1/fs	14 ± 1	16 ± 2	20 ± 2	55 ± 5	406 ± 20	26 ± 2

See also the $\text{Cr}(\text{CO})_6$ τ_1 values for three more wavelengths in Table 2. Error limits are estimated.

(286 nm), near the wavelength (267 nm) used in our previous work [26]; we focused to the early-time behavior, proceeding in the same way as for the chromium carbonyl. Two of the time constants ($\tau_{1\text{old}} = 30$ fs and $\tau_{3\text{old}} = 35$ fs), previously determined also outside the pump–probe overlapping region, are practically confirmed: They are now $\tau_1 = 26$ fs and $\tau_2 = 35$ fs. But $\tau_{2\text{old}}$ (20 fs) must again be replaced by a highly damped oscillation. Its period and dephasing time in L_2 are $\tau_{\text{osc}} = 105$ fs and $\tau_{\text{deph}} = 40$ fs. Remarkably, such an oscillation ($\tau_{\text{osc}} = 108$ fs, $\tau_{\text{deph}} = 34$ fs) can also be detected from the parent ion $\text{Mo}(\text{CO})_6^+$, pointing to a vibration already in the Franck–Condon region L_1 . As above (with the longer wavelengths for $\text{Cr}(\text{CO})_6$), the longer τ_1 provide a better chance to detect a periodic modulation than in the T_{1u} state of $\text{Cr}(\text{CO})_6$ with lifetime 12.5 fs.

$\text{W}(\text{CO})_6$ was not reinvestigated, because already the first time constant ($\tau_1 = 46$ fs) was previously determined outside the pump–probe overlapping time [26]. But we believe that, likewise as in $\text{Cr}(\text{CO})_6$ and $\text{Mo}(\text{CO})_6$, $\tau_{2\text{old}}$ (23 fs) must also be replaced by a highly damped oscillation.

4. Discussion

4.1. Methodology: effective time resolution

Compared with our previous investigation [12], in this work we report about a reduced value for the lifetime of the $\text{Cr}(\text{CO})_6$ Franck–Condon region with 270-nm excitation ($\tau_1 = 12.5$ fs versus $\tau_{1\text{old}} = 23$ fs), although the corresponding value for $\text{Mo}(\text{CO})_6$ ($\tau_1 = 26$ fs versus $\tau_{1\text{old}} = 30$ fs) is practically unchanged. Furthermore, a previous decay with time constant $\tau_{2\text{old}} = 10$ –20 fs is now replaced in all three compounds by a (highly overdamped) high-frequency oscillation. It may well be that this is also the case in the other metal carbonyls ($\text{W}(\text{CO})_6$ [26], $\text{Fe}(\text{CO})_5$ [13], $\text{Ni}(\text{CO})_4$ [14], $\text{Mn}_2(\text{CO})_{10}$ and $\text{Re}_2(\text{CO})_{10}$ [15]) investigated by us. These changes ask for an assessment of the time resolution. In the following, we apply the considerations of [33] to the present case.

The halfwidth of the instrumental function (correlation function of the pump pulse with the third or higher power of the probe pulse), which represents the time resolution, was $\tau_{\text{instr}} = 158$ fs in the previous experiment [12] but in this work $\tau_{\text{instr}} = 32$ fs and 11 fs with the 30-fs and 9.7-fs UV pulses, respectively. However, time resolution is only needed to separate *two* short processes. With sufficient sig-

nal-to-noise ratio, deconvolution with the instrumental function (which must be known) can in principle provide a single time constant, even if it is much shorter than τ_{instr} . (For a complication due to the high probe intensity, see below.) If, for instance, the time constant $\tau \leq 0.1 \times \tau_{\text{instr}}$, this process basically gives rise to a signal with a maximum that is delayed by $\Delta\tau = \tau$, and this can be measured with high accuracy (in our case: 1 fs) due to the monitoring of the time zero by Xe with each laser pulse. Even more than one such time constant can be extracted, if there are several “independent” signals, as demonstrated in many of our previous works (e.g. [34]) and from other labs (e.g. [35]). This can be explained by an analogy:

The satellite Hipparcos localized in 1989–1993 about 120 000 stars with a mean error of 5 nrad [36] which is by a factor of 100 better than the resolution of a telescope with a 1-m mirror (i.e. 1% of the width of the instrumental function). If some of the objects were double stars with an angular separation of e.g. 50 nrad, they were not resolved. But suppose, one of the two stars would emit in the green, the other in the blue range of the spectrum, then the satellite could in principle separate the two in two measurements by detecting with different filters. The number of distinguishable colors would correspond in our case to the number of linearly independent ion signals: If in the simplest case each location gives rise to a signal of its own, the individual $\Delta\tau$ permit to determine each time constant, even if all are only a few percent of τ_{instr} . In general, linearly independent signals (in the linear combination of individual exponentials used to simulate the signals) are sufficient, and curve fitting is used instead of determining $\Delta\tau$. This is a great advantage of having several signals, such as is usual in transient mass spectroscopy.

However, during the pump–probe overlapping time (e.g. near the signal maximum) complications can arise due to the high probe intensity. One source of interference is the additional population of a higher level (around 6 eV) in the substance by absorption of one probe photon (via a virtual level) plus one UV photon; if this level has a longer lifetime, it can influence the temporal signal in an intricate way. In fact, we found a clearly longer time constant (40–55 fs), when we used shorter pump wavelengths (215–196 nm, corresponding to 5.8–6.3 eV, see Section 3.2), suggesting that also a level populated by 1 IR + 1 UV photon in this energy region could have such a lengthened lifetime. We assume that such a real level has influenced the time constant $\tau_{1\text{old}}$ in the previous experiment [11,12], and the deconvolution method resulted in a longer than the real time constant. In molecules, where the real intermediate state is also short-lived (or if there is only a virtual intermediate level), deconvolution can also result in too small time constants; on the other hand, such contributions can often be eliminated (see, e.g. [37]). Such nonlinear effects can be recognized or even eliminated by investigating the dependence on the probe power.

Often also a simple trick helps to avoid such problems: A time constant down to about $\tau = \tau_{\text{instr}}/5$ can be extracted

(if the signal-to-noise ratio is sufficient and if the pulse shapes are well represented by Gaussians over 3 orders of magnitude) by evaluating the signal in the time range of about $5\text{--}8 \times \tau$ (e.g. the range 60–120 fs in Fig. 3a). While the signal is still exponential there, the Gaussian instrumental function has already faded away [33,34]. In this way, evaluation is done outside the pump–probe overlapping time, so that the additional state discussed above is not excited. This method did not work for $\text{Cr}(\text{CO})_6$ in our previous investigation [12], because $\tau_{1\text{old}}$ was too short. But it did work for $\text{Mo}(\text{CO})_6$ (where $\tau_{1\text{old}} = 30$ fs was just at the mentioned limit) and $\text{W}(\text{CO})_6$ ($\tau_{1\text{old}} = 46$ fs), and both values were also derived from the shift of the signal maximum [12,15,33]. In the present work, we checked the first time for $\text{Mo}(\text{CO})_6$ and found $\tau_1 = 26$ fs, which agrees with the previous value within the error limit.

We conclude that one can extract time constants that are shorter than the time resolution (e.g. 20% of τ_{instr}), even several such constants under favorable conditions (if there are linearly independent signals). It is preferable to deduce them outside the pump–probe overlapping time. Constants derived from deconvolution during this time must be checked for contribution by nonlinear effects. However, whereas time constants shorter than τ_{instr} can be determined, one does need the corresponding resolution and short pulses to detect a high-frequency oscillation. Pulses that are longer than a period would simply average over the signal.

In the previous work [11,12], we thought to recognize an exponential relaxation with time constant $\tau_{2\text{old}}$ (10, 20 and 23 fs for the carbonyls of Cr, Mo and W) taking place before dissociation. It was deduced by comparing the measured signal with a simulated one, using decays with time constants $\tau_{1\text{old}}$, $\tau_{3\text{old}}$, $\tau_{4\text{old}}$, etc. With the better resolution in the present work, one can recognize that this deviation is not purely exponential, but shows a modulation, namely a highly damped oscillation. It must be due to vibrational modulation of ${}^n\sigma_i$ with $n = 5$ and 4 (i.e. in the signals $\text{Cr}(\text{CO})_5^+$ and $\text{Cr}(\text{CO})_4^+$). Because the location L_1 only gives rise to $\text{Cr}(\text{CO})_6^+$, the vibration must come from L_2 (which would be $L_{3\text{old}}$). (L_3 is only populated after the decay of this oscillation.) The pure dephasing time τ_{deph} (defined in Eq. (2)) is 30 fs. Multiplication of the oscillatory function (Eqs. (1) and (2)) by the decaying L_2 population results in a signal component with decay time $\tau_d = (\tau_{\text{deph}}^{-1} + \tau_2^{-1})^{-1} = 11$ fs. If the periodic modulation would not be resolved, this component would represent an exponential decay with time constant τ_d . It is therefore very satisfactory that practically $\tau_d = \tau_{2\text{old}}$.

4.2. Survey of the assignment of lifetimes and oscillations

The assignment was discussed in detail in our previous work [12]. The steps in the dissociation product $\text{M}(\text{CO})_5$ were confirmed by high-level calculations [22,23]. Therefore we give here only a brief survey. To facilitate discussion, we show schematic potentials in Fig. 7. Details will be presented in the next section.

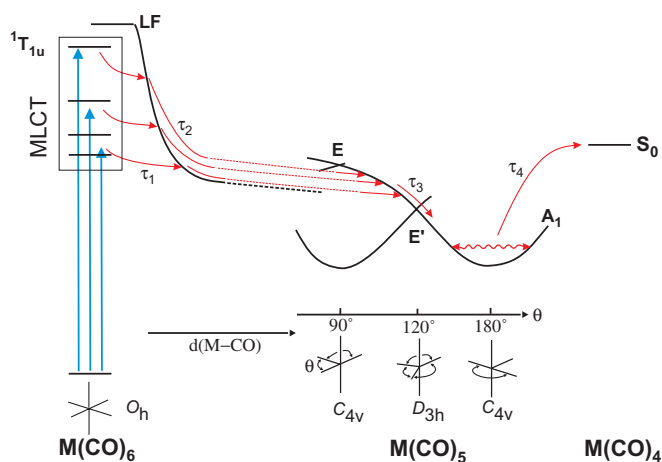


Fig. 7. Schematic potentials and dynamics, using three different pump wavelengths (270, 318 and 345 nm), which initially excite MLCT states (T_{1u} with 270 nm). The initial relaxation (during slightly different times τ_1) follows MC stretch and JT-active coordinates on potentials as suggested in Fig. 8, from where the wave packet crosses over to the lowest LF surface. On this surface, the trajectories are probably still separate (during τ_2), merging only above the conical intersection (CI) in the dissociation product $\text{M}(\text{CO})_5$. During τ_2 , the MC distance increases much less than indicated in the figure (broken lines) for clarity. After passing the CI (within τ_3), the wave packet oscillates in the C_{4v} minima along the pseudorotation coordinates indicated at the bottom; there are three symmetry-equivalent such minima around each D_{3h} CI (see the drawing in [12]). The MC stretch oscillation (observed in all L_i) is not indicated. Further dissociation to $\text{M}(\text{CO})_4$ (within τ_4) is promoted by excess energy.

For assignment of the τ_i and ${}^n\sigma_i$ (Tables 1 and 2) and hence the identification of the L_i , it helps to know that the degree of fragmentation increases (i.e. the mass of the maximum signal decreases) with increasing i , as illustrated in Fig. 2. This is because in this sequence, more and more electronic energy is converted to kinetic energy of the nuclei; vertical ionization from such a hot neutral then generates a hot ion, which subsequently has sufficient time (many nanoseconds, early during acceleration in the ion source) to fragment [34]. Consequently, the intensity of the parent ion $\text{Cr}(\text{CO})_6^+$ is largest in the Franck–Condon region ($i = 1$), whereas the final product (L_5) (recognizable from its “infinite” (>500 ps) lifetime) gives rise to small-mass signals only. In the given case of $\text{M}(\text{CO})_6$, the assignments in the previous experiment [12] and the calculations [22,23] can also point to the assignment in particular of the later steps. The final time constant τ_4 (for the process $L_4 \rightarrow L_5$) of around 1 ps slightly depends on the excitation wavelength (Table 2) and thus on the excess energy in L_4 ; hence it is probably a ground-state process, probably $\text{M}(\text{CO})_5 \rightarrow \text{M}(\text{CO})_4$, as indicated in Fig. 7. In fact, this process is observed in the gas phase and is suppressed in solution [38–41], and τ_4 is the only time that is long enough that cooling by the solvent can prevent the reaction. L_4 can also be identified as (the ground state of) $\text{M}(\text{CO})_5$ (and not a smaller fragment) by the oscillations observed there: These oscillations have the same frequency in all signals $\text{M}(\text{CO})_n^+$ with $n = 0, \dots, 5$ ($n = 0, \dots, 4$ for $\text{M} = \text{Cr}$; but

note that the ion $\text{Cr}(\text{CO})_5^+$ is lost already with very minor excess energy due to its extremely small dissociation barrier [12]; hence they are all due to a single neutral species $\text{M}(\text{CO})_n$ with $n \geq 5$. Actually, $n = 6$ can be excluded, because it is known that dissociation does occur.

The preceding step (τ_3) was already previously [12] assigned to the lifetime of the first excited singlet state S_1 of $\text{M}(\text{CO})_5$, which is depleted to S_0 via a Jahn–Teller induced conical intersection (Fig. 7). The idea of initial population of S_1 was based on a correlation argument and the observation of luminescence after dissociation of nickel carbonyl. The assumption lead to an easy rationalization of the oscillations in L_4 : They are driven by the slope on leaving from the conical intersection; the vibrational coordinate is hence expected – and found – to coincide with the Jahn–Teller active coordinates. These processes have all been confirmed by calculation [22,23]. The preceding step (τ_2) must then represent the dissociation itself (Fig. 7), and τ_1 must be the relaxation out of the Franck–Condon region in the intact molecule.

The oscillations can be easily identified by their frequencies: The higher wavenumbers ($350\text{--}450\text{ cm}^{-1}$) are in the range, where only MC stretch vibrations are observed in metal carbonyls (see, e.g. [42]). Selection rules suggest that it is the totally symmetric one of them. The lower wavenumber ($80\text{--}95\text{ cm}^{-1}$), observed only in the dissociation product $\text{M}(\text{CO})_5$, is in the range of CMC bending vibrations [42]. In D_{3h} (symmetry at the conical intersection) there are only two such vibrations (both degenerate, e' , one involving the axial and the other the equatorial ligands); they are JT active. In the symmetry (C_{4v}) of the S_0 minima they decompose into $e + a_1 + b_2$, the degenerate one involving the axial ligand and the latter two corresponding to pseudorotation of the ligands in the basal plane. It was suggested in [12] and confirmed in [22,23] that the observed oscillation just correspond to this pseudorotation in $\text{M}(\text{CO})_5$ (Fig. 7); it is expected to be the totally symmetric component (a_1 in C_{4v}) of it.

4.3. The individual steps on the potential

4.3.1. Relaxation out of the Franck–Condon region (τ_1)

Since the work of the Pierloot and Baerends groups [4–7], there is agreement that most LF states lie above the MLCT states in $\text{M}(\text{CO})_6$. In the near UV, practically only the latter are excited, also because LF states e.g. near 250 nm, indicated in Fig. 1, have a much smaller oscillator strength than the MLCT states according to [43]. (There is still a discussion [8], whether also triplet states are populated by optical absorption. This possibility is, however, rejected in Sections 1 and 5.) The – repulsive – LF states energetically steeply fall down along the metal–carbon stretch coordinate, whereas the MLCT states are primarily not dissociative, because they correlate with charge-separated products. However, an avoided crossing with the LF curves can give rise to a minor or even vanishing barrier, over which the initial MLCT population can reach

the dissociative curve [4–6]. The dissociation is hence not direct, but requires a crossing-over to an LF potential surface. This seems to be in full agreement with our observation, that a relaxation step (within τ_1) precedes the actual dissociation (within τ_2).

A closer investigation of the energies along the M–C stretch coordinate by time-dependent density functional theory, however, suggested that basically only one repulsive curve results from this mechanism, starting from one (or two) of the lowest MLCT states (T_{2u} , which can mix with E_u), whereas the other MLCT states seem to be bound [4–6]. This is shown in Fig. 8a, which is adapted from [4]. How does then, for instance, the T_{1u} population (excited at 270–282 nm) find the repulsive curve within 12.5 fs? Such a short time obviously requires a very rapid acceleration and hence a very steep initial down-slope. We suggested already in [11,12] that such a slope exists along Jahn–Teller (JT) active coordinates. This is shown in Fig. 8b. The JT-induced crossings can provide an ultrafast path, for example, from T_{1u} down to T_{2u} , from where population could flow to the repulsive LF state [11,12]. This mechanism would thus follow the Kasha rule, saying that the molecule first relaxes down to S_1 before reaction [44] (or radiation [45]) takes place. However, if the time τ_1 represents $T_{1u} \rightarrow T_{2u}$ relaxation, this step should not exist on direct excitation of T_{2u} at 318 or 345 nm (whatever is the spectral assignment, see Fig. 1), which is in contrast to our observation (Table 2). Is there hence a direct (“anti-Kasha”) path from each MLCT state to a repulsive LF surface, τ_1 representing this step?

We suggest that this is indeed the case, although details may be more complicated. One should notice that Fig. 8a only shows the (lowest) MLCT curves and that in density functional theory, on which Fig. 8a is based, the lowest LF state (T_{1g}) is below the T_{1u} state [4]. In the more accurate CASPT2 calculations, T_{1g} is slightly above T_{1u} [7,8]. Both states split along the MC stretch coordinate to an E and an A_1 state (in C_{4v}), which will lead to an avoided crossing similar as with the lower T_{2u} state. We thus suggest that the E state rising from T_{1u} in Fig. 8a is caused in this calculation by repulsion from the E state resulting from the lower-lying T_{1g} state. If T_{1u} and T_{1g} are interchanged, one can expect a declining E curve resulting from T_{1u} and an E curve from T_{1g} (that is steeper) as sketched in Fig. 8c versus MC stretching. Also versus the JT-active e_g MC stretching one obtains a declining E curve from T_{1u} and other triply degenerate states. With this model, there is a direct (anti-Kasha) MLCT \rightarrow LF relaxation from T_{1u} via the curve crossing (actually: avoided crossing) as indicated in Fig. 8c. From the higher T_{1u} state (excited at 224 nm), the same LF state can be reached in a different direction, namely along JT-active coordinates (Fig. 8b). While this path resembles our previous suggestion [11,12], it represents again a direct MLCT \rightarrow LF relaxation. The model hence says that on T_{1u} excitation (270–290 or 224 nm) the intact molecule does not reach S_1 but dissociates before. It should further be noted that distortion along

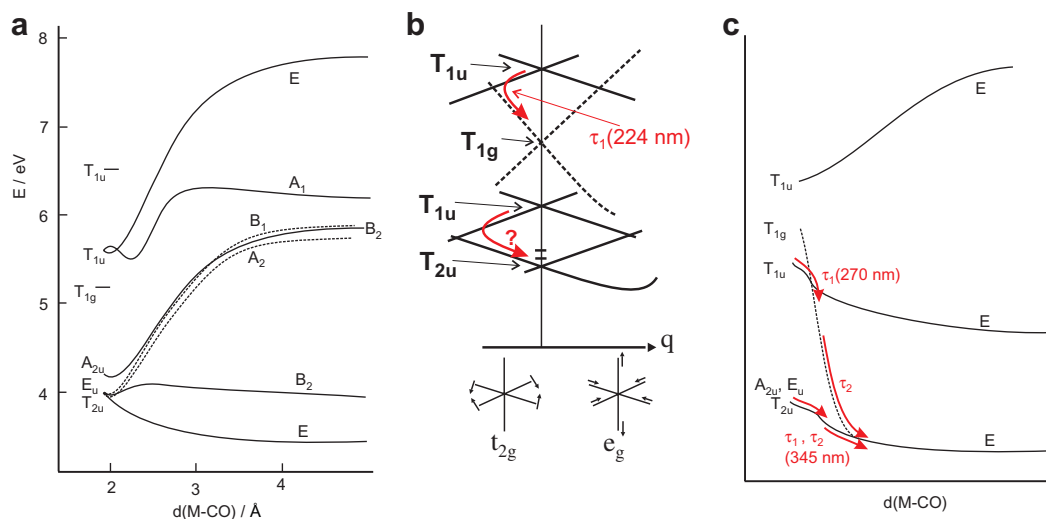


Fig. 8. (a) Potential-energy curves along the Cr–CO stretch coordinate according to [4]. (b) Simplified potential-energy curves along Jahn–Teller active coordinates (t_{2g} or e_g), that can provide paths for ultrafast relaxation to lower states. Note: a t_{2g} distortion actually splits the triply degenerate states into three (in D_{2h}), an e_g distortion initially into two (in C_{4v}), of which the degenerate one later splits again. (c) Potentials (shown are only the E states in C_{4v}) along the Cr–CO stretch coordinate, modified: Compared to (a), the LF state T_{1g} has been placed above the lowest T_{1u} state. Potentials correlating with T_{1g} are indicated by broken lines; but note that at larger MC distance all repulsive potentials have LF character. Also note that the crossing of the T_{1u} and T_{1g} curves is actually avoided in the drawing plane.

JT-active coordinates (e_g MC stretching and t_{2g} MCO bending) also mixes the different MLCT states. In fact, vibronic interaction between them must be strong. This is implied by the not very different oscillator strengths of allowed and forbidden bands (Fig. 1), indicating strong intensity borrowing. Strong vibronic interaction points to the neighborhood of a conical intersection (CI), and a CI can usually provide an ultrafast path from a (in this case: slightly) higher to a lower state, e.g. from A_{2u} to T_{2u} .

To summarize this part: A direct and fast path seems to exist from every MLCT state to a repulsive LF state. There seems to be no need for a preceding relaxation down to T_{2u} – or it is just not fast enough to compete –, although this path certainly also exists and is barrierless, made possible by JT-induced conical intersections [12]. The choice between the two paths is probably controlled by the relative slopes. Distortions providing the required steep down-slopes for the MLCT \rightarrow LF relaxation are in some cases simple MC stretching (which can be considered as a superposition of a_{1g} , e_g and t_{1u} stretching), whereas in other cases Jahn–Teller active coordinates (e_g MC stretching and t_{2g} MCO bending) are involved. Such distortions also mix the MLCT states. We suggest that τ_1 is the time constant for MLCT \rightarrow LF relaxation in all cases. Where this path involves intermediate mixing-in of additional states, the probing technique seems not to distinguish such components. We also point out that this model is consistent with the rapid change of fragmentation (only the parent ion from L_1 , no parent ion from L_2): The ultrashort τ_1 times imply a fast acceleration and hence a steep initial slope; the rapid lowering of the electronic energy gives rise to excess kinetic energy of the nuclei, which in the ion causes efficient fragmentation. If the time constants are controlled

by the initial accelerations and slopes, and also by the height or absence of a barrier resulting from an avoided crossing, it seems natural that they are characteristic of each state and that the wavelength dependence can be non-monotonic, as we observed (Tables 2 and 2a). In contrast, in a statistical model the lifetimes would monotonically decrease with increasing excess energy. By far the longest τ_1 is observed at 162 nm, which probably excites a Rydberg state. Its potential (resembling that of a $\text{Cr}(\text{CO})_6^+$ ion in its T_{2g} ground state) is not expected to be repulsive, and the repulsive valence states are much lower in energy; an intersection or avoided crossing between the two types of potential may therefore be far from the Rydberg minimum and involve some activation energy.

The model suggests the expected relaxation coordinates. Information on these initial coordinates can be derived from resonance Raman spectra. With a number of different pump wavelengths between 355 and 213 nm, activity was in fact found in JT-active e_g and t_{2g} modes in $\text{Cr}(\text{CO})_6$ and $\text{W}(\text{CO})_6$ [46–48]. This confirms our suggestion above, that they are components of the direction of the initial slope. With 266 nm, also t_{1u} and t_{2u} overtones were found and interpreted as an indication of vibronic mixing of LF and MLCT states [46,49]. (In this energetic region an LF state is expected (Fig. 1). It is probably not directly excited, because the absorption is expected to be too weak [43].) A remarkable finding is that all the vibrational progressions were found to be very short (up to the first overtone; only traces of higher ones detected in [47]) [46–49], in stark contrast to other dissociating molecules [50]. This was interpreted in [46] in terms of an upper-state potential that is nearly not shifted versus the equilibrium geometry. However, this is incompatible with the ultrashort τ_1 values

found here, implying a very fast acceleration and a steep initial slope. We instead infer from the short progressions that the wave packet leaves the initially excited state very early (within τ_1) to a potential surface (such as an LF surface), from where transition to S_0 involves a much smaller transition moment. This again confirms our model. (To explain the short progressions, Adelman and Gerrity [46] also offered intersystem crossing. This was, however, excluded in [12], because all time constants were found to be longer with the heavier metal. See also Sections 1 and 5.)

A support for a specific JT-active mode (t_{2g} , which is an MCO bending coordinate) is due to photofragment spectroscopy, in which rotationally excited CO was found after photodissociation of $\text{Cr}(\text{CO})_6$ [51–53]. This observation indicates a bent MCO structure before dissociation, so that the recoil can excite rotation. Such a bending can be provided by a t_{2g} deformation [12].

The time τ_1 is amazingly short (12.5 fs with 270 nm or 14 fs with 282 nm). This can be judged by comparison with a motion in a bound potential, for example along an MC stretch coordinate with vibrational wavenumber 400 cm^{-1} . To travel from any point on the slope of this potential to its minimum (or a point close-by, where it might find an outlet – a CI or an avoided crossing – to another potential), a wave packet needs one quarter of a period, hence 20 fs. At the Franck–Condon point with its O_h symmetry, the only coordinates with nonzero slope are either totally symmetric (a_{1g}) or JT active. Along the a_{1g} MC stretching, six MC bonds are extended in phase and the potential in this direction is bound; its curvature corresponds to a vibrational wavenumber of 360 cm^{-1} (period 93 fs, Section 4.4). Traveling to its minimum would thus take 23 fs, longer than observed (12.5 fs) in $\text{Cr}(\text{CO})_6$. For the JT-active MC stretch mode (e_g) a similar wavenumber is expected, as to judge from the ground state [42]. In contrast, a higher frequency is expected for the JT-active MCO bending (t_{2g} , 532 cm^{-1} in S_0 [42], 15 fs for a quarter of a period). Therefore we suggest that excursion along this direction significantly contributes to initial acceleration and transition to the LF state (which agrees with the evidence from CO rotational excitation in photofragment spectroscopy, see above). Later on, an ungerade direction such as t_{1u} must mix in, since gerade coordinates would not lead to dissociation, because they involve more than one ligand. (A local MC stretch is a superposition of t_{1u} with e_g and a_{1g} MC stretch coordinates.) u-type distortion breaks the inversion symmetry, which is also necessary to permit transition from an MLCT state (u symmetry) to an LS potential (g symmetry).

4.3.2. The dissociation step (τ_2)

After crossing over to the lowest LF potential surface (symmetry type T_{1g} in O_h), the MC bond is extended and the state splits. The wave packet follows the lower one (E symmetry in C_{4v}) and within τ_2 arrives at the S_1 state of E symmetry of $\text{M}(\text{CO})_5$. The dissociation is remarkably fast ($\tau_2 = 18\text{--}22$ fs, Table 2), probably the fastest measured

to date by time resolution. From photofragment spectroscopy of $\text{W}(\text{CO})_6$, excited at 351 nm, it is known that CO is ejected with a translational temperature of 1550 K [52], corresponding to a mean square velocity of 1170 m s^{-1} . With this velocity, the MC distance can increase within τ_2 by only 0.23 Å (or half as much, assuming uniform acceleration). This should be compared with the Cr–CO bond length of 1.92 Å (see [54] and references quoted therein) in $\text{Cr}(\text{CO})_6$. This means that the energy of the lowest LF states falls down very steeply (“precipitously” [4]) to near the final level by extending the MC bond by only 10%. This is in agreement with the early (within τ_1) crossing-over to this surface and the fact that τ_1 and τ_2 increase only slightly on lowering the initial excitation energy. It is also consistent with the very short progressions in resonance Raman spectra (Section 4.3.1).

Another remarkable fact is the energetics: The Cr–CO bond dissociation, leading to $\text{Cr}(\text{CO})_5$ in its C_{4v} ground state, requires 1.6 eV (see Table 8 in [55] and references quoted). Vertical excitation of $\text{Cr}(\text{CO})_5$ (in a Ne matrix) requires 1.95 eV [56], so that the Franck–Condon (FC) point of this unsaturated carbonyl is by 3.55 eV above the hexacarbonyl ground state. On the other hand, the long-wavelength absorption edge (375 nm) corresponds to only 3.3 eV; similarly our longest pump wavelength (345 nm, 3.6 eV) combined with the steep initial slope will not allow the wave packet to reach the FC region of $\text{Cr}(\text{CO})_5$. For explanation we again invoke the JT effect: Paterson et al. [22] point out that already with minor extension of the Cr–CO bond the E state resulting from splitting of the T_{1g} state is again split by the JT effect (by 0.86 eV [22]), giving rise to symmetry-equivalent valleys down to the S_1 surface of $\text{Cr}(\text{CO})_5$; these curves thus do not lead to the FC point (which is the E state of the nondistorted pentacarbonyl). The JT active coordinates should be CMC bending of b_1 and b_2 symmetry, the latter probably more effective. This b_2 deformation is the same as a component leading in $\text{Cr}(\text{CO})_5$ from the FC point down to the conical intersection with trigonal-bipyramidal structure. Hence these valleys lead to an energy lower than the FC point in $\text{Cr}(\text{CO})_5$. Therefore also long-wavelength excitation of $\text{Cr}(\text{CO})_6$ can reach the excited state of the pentacarbonyl. We hence suggest that the paths starting from the different initial states go down on the same LF surface, although with longer wavelengths the trajectories lie deeper in the valleys leading closer to the CI in $\text{M}(\text{CO})_5$ (Fig. 7). A nice confirmation of this idea can be seen in the S_1 lifetimes (τ_3) of $\text{Cr}(\text{CO})_5$ (Table 2), which decrease with longer pump wavelength: the traveling distance to the CI is shorter in this case. Lifetimes that are shorter with less excess energy are probably hard to rationalize in a different way.

4.3.3. The S_1 lifetime of $\text{M}(\text{CO})_5$ (τ_3)

The short τ_3 (Table 2) implies a barrierless continuous path down to S_0 . As mentioned in Section 4.2 and explained previously [12] and confirmed by calculations [22,23], a suitable conical intersection (CI) is available with

trigonal-bipyramidal molecule structure (symmetry D_{3h}); it is induced by the JT effect. The JT-active coordinates correspond to CMC bending (symmetry e' in D_{3h} , $a_1 + b_2$ in C_{4v}), which basically exchange the ligand vacancy (in square-pyramidal geometry) with an adjacent CO group (pseudorotation). After passing through the CI, the wave packet oscillates in S_0 (i.e. in L_4) along the pseudorotation coordinate with a period of 350 fs ($\text{Cr}(\text{CO})_5$). In a quarter of this period (in 88 fs) the wave packet should travel from the point of maximum amplitude (turning point) to the minimum. The question is then: Why is τ_3 much shorter (40–25 fs), although the coordinate is the same? We suggest that this is because (1) the wave packet arrives in S_1 not at the FC point (i.e. above the S_0 minimum) but closer to the CI and (2) arrives there already with a b_2 momentum acquired before (by the JT effect on the repulsive curve, Section 4.3.2).

4.3.4. Further dissociation from pentacarbonyl S_0 (τ_4)

It was already argued in [12] that the time for dissociation ($\tau_4 \approx 1$ ps) is shorter than statistically expected with the excess energy from 270-nm dissociation. Apparently, compared with equipartition, a larger fraction of the energy seems to be in suitable stretch coordinates. A non-statistical energy distribution is, of course, also required for the coherent oscillations observed. It is consistent with this non-equipartition situation, that τ_4 only increases from 0.93 to 1.5 ps (Table 2) on decreasing the excess energy by 1.0 eV (increasing the pump wavelength from 270 to 345 nm).

4.4. Coherent oscillations

Already in our previous work [11,12], we found coherent oscillations after dissociation, in the ground singlet state of $\text{M}(\text{CO})_5$ (wavenumbers 95, 84 and 80 cm^{-1} for $\text{M} = \text{Cr}$, Mo and W , respectively). They were identified with pseudorotation vibrations in a C_{4v} minimum, obviously stimulated by the slope down from the conical intersection with D_{3h} symmetry, as also confirmed by the calculations by Paterson, Worth et al. [22,23]. They are found again

in the present work, and a closer inspection reveals more details, which will be reported later.

With the better time resolution, we now also detect a higher-frequency oscillation, also in the preceding locations (Table 3). From its wavenumbers around 400 cm^{-1} , it can only be an MC stretch vibration. It is certainly totally symmetric (a_{1g} “breathing” in O_h , a_1 in C_{4v} , etc.), because from antisymmetric vibrations one in general only observes overtones [57]. This vibration is already found in the FC region (L_1) of $\text{Mo}(\text{CO})_6$, excited at 270 nm, and with longer-wavelength excitation also in L_1 of $\text{Cr}(\text{CO})_6$. Obviously with 270 nm, in this molecule τ_1 (12.5 fs) is a too small fraction of the period (80–100 fs) to allow detection of a such a modulation. Indeed this vibration was also detected in static spectroscopy in a cryogenic matrix as vibrational structure in the T_{1u} band of the molybdenum and tungsten carbonyls (wavenumbers ≈ 350 and ≈ 400 cm^{-1} , respectively) but not in chromium carbonyl [58], certainly for the same reason. The wavenumber observed in the time-resolved experiment of $\text{Mo}(\text{CO})_6$ (310 cm^{-1}) is – in view of the error limit caused by the short lifetime – in satisfactory agreement with the former value. Coherent oscillations in the FC region can be stimulated, if the pump laser’s coherent width covers more than one of the stationary vibrational levels. Already the width of the 30-fs laser (490 cm^{-1} full width at half maximum) is sufficient.

The MC stretch vibration is seen as a coherent oscillation also in the subsequent locations L_2 – L_4 on the potentials of $\text{Cr}(\text{CO})_6$, although with different frequencies. In particular for L_2 , a periodic motion in MC direction seems surprising at first sight, because L_2 was described above as a potential that is strongly repulsive in MC stretch direction. A down-slope along this direction was also postulated for L_1 in Section 4.3.1. However, the vibration takes place along an a_{1g} direction, involving in-phase stretching of six MC bonds, which does not lead to dissociation. The symmetric vibration is schematically illustrated in Fig. 9, which also shows two of the channels for dissociation; the latter follow the bottom of the valley, whereas the vibration is orthogonal to this direction. This is similar as the coherent

Table 3
Fast oscillations (period τ_{osc} corresponding to wavenumber ν , dephasing time τ_{deph} , phase delay φ ; see Eq. (2)) observed in the different observation windows L_i

$\lambda_{\text{pump}}/\text{nm}$	L_1			L_2			L_3			L_4		
	$\tau_{\text{osc}}/\text{fs}$	$\tau_{\text{deph}}/\text{fs}$	$\varphi/2\pi$	$\tau_{\text{osc}}/\text{fs}$	$\tau_{\text{deph}}/\text{fs}$	$\varphi/2\pi$	$\tau_{\text{osc}}/\text{fs}$	$\tau_{\text{deph}}/\text{fs}$	$\varphi/2\pi$	$\tau_{\text{osc}}/\text{fs}$	$\tau_{\text{deph}}/\text{fs}$	$\varphi/2\pi$
270	–	–		93 ± 10	27 ± 10	0.58 ± 0.05	73 ± 10	37 ± 10	0.88 ± 0.05	95 ± 3	165 ± 50	0.67 ± 0.05
318	86.5 ± 15	150 ± 100	0.36 ± 0.10	93 ± 10	76 ± 20	0.52 ± 0.05	73 ± 10	40 ± 10	0.9 ± 0.05	95 ± 5	200 ± 50	0.6 ± 0.05
345	86.5 ± 15	200 ± 100	0.36 ± 0.10	93 ± 10	70 ± 30	0.66 ± 0.05	73 ± 10	40 ± 10	0.16 ± 0.05	95 ± 7	270 ± 50	0.58 ± 0.05
ν/cm^{-1} at 270– 345	397 ± 69			362 ± 39			465 ± 64			352 ± 26		

Error limits indicate the range, in which reasonably good fits are possible.

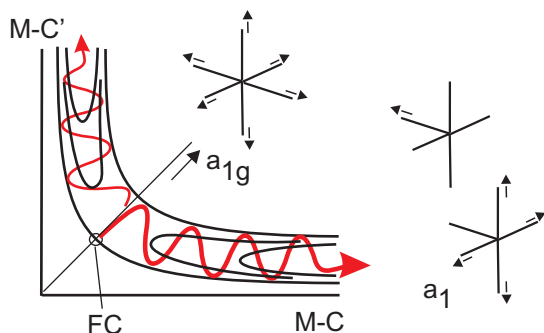


Fig. 9. The totally symmetric (breathing) MC stretch a_{1g} in $M(CO)_6$, stimulated at the Franck–Condon (FC) point and transforming along localized M–C dissociation coordinates into two a_1 vibrations in $M(CO)_5$.

HgI oscillation found in the early time of femtosecond chemistry by the Zewail group in HgI_2 dissociation [59,60].

In a previous experiment on $CpMn(CO)_3$ (Cp = cyclopentadienyl) an observed oscillation (period 85 fs) was assigned to a vibration (wavenumber 392 cm^{-1}) of a local MC bond along the dissociation coordinate [61,62]. In fact it is conceivable that this molecule is different from ours, since the (supposed) dissociation time (170 fs) is much longer and a barrier was suggested along the path. However, a totally symmetric MC vibration, excited by the pump laser in the Franck–Condon region, seems to us also plausible for this case.

As already said, the vibration also survives in the following locations and was monitored for the chromium carbonyl system down to S_0 of the dissociation product (i.e. L_4). (The wavenumber of 350 cm^{-1} , observed by us in this state, compares favorably with the 381 cm^{-1} , observed for the solvent complex $Cr(CO)_5 \cdot \text{cyclohexane}$ [48].) On a change of the electronic state, it substantially changes its frequency (by 20%, Table 3). Normally such a change leads to rapid dephasing of the coherent motion. However, all the relaxations take place in times ($\tau_1 - \tau_3$) shorter than a period, so that dephasing cannot fully develop. But such an effect can be the reason, why in L_4 (ground state of $Cr(CO)_5$) the dephasing time of this vibration (165–270 fs) is much shorter than that of the lower-frequency vibration ($>1\text{ ps}$), which is only excited on the lower surface: The a_1 vibration changes by 20% (from 450 to 350 cm^{-1}) on $S_1 \rightarrow S_0$ ($L_3 \rightarrow L_4$) relaxation, so that after a small multiple of the vibrational period (74 fs in S_1) the two vibrations will be out of phase. Another possible source of dephasing is connected with the following observation.

In the simulation of the 318-nm and 345-nm data, we fixed the frequencies for the oscillations in L_3 and L_4 to the values found with 270-nm pump. This idea is based on the model (Sections 4.3.2 and 4.3.3) saying that in all cases dissociation leads to S_1 (i.e. L_3) and then S_0 (L_4) of $Cr(CO)_5$, and vibrations in these electronic states should only slightly depend on the excess energy, due to anharmonicity. However, releasing this constraint for L_2 – L_4 in the

simulations results in slightly better fits with frequencies that are by about 10% lower with lower excess energy (longer wavelengths). Anharmonicity usually gives rise to the opposite result. An explanation may be provided by the existence of two a_1 MC stretch vibrations (for the axial and equatorial bonds), whose frequencies are likely to be slightly different. Their superposition would then shorten the dephasing time. At longer wavelength, the lower frequency seems to be favored. This means also less superposition and hence a longer dephasing time; this is indeed found at longer wavelengths (Table 3).

The phases φ of the oscillations are also reported in Table 3. They should monotonically increase in the model that the oscillations simply propagate from location to location (as in Fig. 9). In fact, the data are consistent with a monotonic increase, if one takes into account that φ is defined only up to modulo 2π . An alternative to propagating oscillations, excited in the FC region, postulates restimulation of MC stretch vibration on each crossing-over to a new electronic state, by which the MC vibrational frequency or the bond length is suddenly changed. In fact, the MC stretch vibration was found oscillating in S_0 of $Cr(CO)_5$ in the quantum dynamics simulation [23], that started from the S_1 of this molecule (i.e. not from the FC region of $Cr(CO)_6$).

It seems remarkable that the S_1 state of $Cr(CO)_5$ (which is an LF state) has a larger wavenumber (450 cm^{-1} , Table 3) of the MC stretch vibration than usual. This observation still awaits electronic interpretation. But it might also have to do with the existence of two a'_1 (or a_1) vibrations, one of them preferred in the higher state and the other in the lower one.

5. Conclusion

By the better time resolution in the present work as compared to the previous investigation [12], we found that the previously supposed second relaxation step in the intact $M(CO)_6$ (with time constant $\tau_{2\text{old}} = 10$ – 20 fs) is not purely exponential but contains a periodic modulation. It corresponds to a totally symmetric MC stretch vibration, taking place during dissociation of a single MC bond. It is already excited in the Franck–Condon region by the pump laser and seems to propagate over four electronic levels down to the ground state of the dissociation product $M(CO)_5$, although restimulation by a changed MC distance or slope on transition to a new electronic state may also contribute. By contrast, a lower-frequency coherent oscillation appears only after the molecule reaches a minimum of C_{4v} symmetry (square-pyramidal geometry) in $M(CO)_5$. It is assigned to a totally symmetric CMC bending vibration that is associated with pseudorotation and is stimulated by the slope on entering this potential well from the S_1/S_0 conical intersection with trigonal-bipyramidal molecule geometry. That is, in contrast to the higher-frequency vibration which is (mainly) optically induced, the pseudorotation vibration is chemically induced. A strong support are the recent cal-

culations [22,23], which predict such a vibration without any counterpart in a preceding electronic state. (The calculation of Worth et al. [23] suggests that also the MC vibration in part is stimulated by a bond length change on changing the electronic states.) Chemically induced vibrations can be very useful to find out the directions of slopes and hence information about the reaction coordinates. Except for the metal carbonyls [11–15], we have demonstrated this principle with aminobenzonitriles [57,63–65] and with tetrafluoroethylene [32]. A chemically induced coherent oscillation was also detected by Sorgues et al. in a tetraamino ethylene [66]. A previous theoretical work assumes that there exist only optically induced coherent oscillations [67].

The new data suggest some modifications of the early phases of the dissociation dynamics: Previously [12] we said that from the initial MLCT state T_{1u} excited at 270 nm, the molecule relaxes down to one of the lowest singlet states (T_{2u}) in an ultrashort time (τ_1), guided by steep slopes induced by the Jahn–Teller effect, and from there reaches a repulsive LF state via an avoided crossing. While a barrierless path of this kind probably exists for all MLCT states, we now suggest that along the JT-active and/or MC stretch coordinates there is an even faster path for all MLCT states directly to the repulsive LF surface. A detour via T_{2u} is not necessary. The previous mechanism had some similarity with the Kasha rule, with the paths from different initial states merging within the intact molecule. In the new mechanism, the different trajectories merge only in the product $M(CO)_5$, at or just above its S_1/S_0 conical intersection. The necessary structural change (CMC bend similar to pseudorotation in $M(CO)_5$) already begins early during dissociation by JT distortion of the molecule in the E state. This mechanism also explains, why photodissociation at the long-wavelength edge of $M(CO)_6$ can still produce the excited singlet state (although not in its FC region) of $M(CO)_5$.

This latter observation also implies that the long-wavelength wing of the $M(CO)_6$ spectra do not reflect singlet–triplet transitions, in contrast to the early [68] and a very recent [8] suggestion and the assignment in textbooks [2,19]. One can also rule out intersystem crossing, that would produce triplets from initial singlets still in the intact molecule; it was also assumed in textbooks [2,19]. We already excluded it previously [12], because all the measured time constants are longer in the heavier $M(CO)_6$, whereas spin–orbit coupling would imply an opposite trend. From an experiment with much less time resolution, Joly and Nelson already concluded that dissociation takes place in the singlet manifold [49].

It may be worth pointing out that in this mechanism (as also in the previous one), the molecule or wave packet is guided by the slopes and intersections of potential surfaces (“pathway approach” [69]). Also the choice between the two paths – direct MLCT \rightarrow LF crossing-over (favored in this work) versus a preceding (Kasha-like) down-relaxation to T_{2u} – is probably decided by relative slopes. In contrast,

the traditional assumption involved vertical relaxation among excited states, guided by matrix elements and densities of states (see the discussion in [70] or pages 458–462 of [71]), reaching equipartition of the energetically accessible states. Such a statistical situation is also excluded by the coherent phenomena (oscillations) observed here.

Although the dissociation of $M(CO)_6$ is indirect (i.e. the repulsive potential is reached only after a preceding relaxation step), the observed duration for it (whether one takes $\tau_1 + \tau_2$ or only τ_2) is to our knowledge the shortest time for dissociation observed so far in time-resolved experiments. We are not aware of a successful time-resolution of a direct dissociation such as that of methyl iodide excited in the A band. The latter process has been estimated to take $\tau_{diss} \leq 65$ fs from the rotational anisotropy in photofragment spectroscopy [72]. But our results also provide an estimate for such processes: The evolution time on the repulsive surface until MC dissociation ($\tau_2 = 18$ –30 fs for the different metal carbonyls) is about one quarter of the period of a typical MC vibration. This is four times shorter than previously supposed (e.g. for CH_3I in [73]). If this rule is general, we can expect $\tau_{diss} \approx 15$ fs for CH_3I (which has a CI stretch wavenumber of 533 cm^{-1} [74]) and around 4 fs for HI (stretch vibration 2300 cm^{-1} [75]).

Acknowledgments

This work was supported by the Deutsche Forschungsgemeinschaft (project FU 363/1) and the European Union’s Human Potential Program under Contract MRTN-CT-2003-505138 (XTRA).

Appendix A. Supplementary data

Supplementary data associated with this article can be found, in the online version, at [doi:10.1016/j.chemphys.2007.09.057](https://doi.org/10.1016/j.chemphys.2007.09.057).

References

- [1] M.S. Wrighton, Chem. Rev. 74 (1974) 401.
- [2] G.L. Geoffroy, M.S. Wrighton, Organometallic Photochemistry, Academic Press, New York, 1979.
- [3] S.A. Mcgregor, O. Eisenstein, M.K. Whittlesey, R.N. Perutz, J. Chem. Soc., Dalton Trans. (1998) 291.
- [4] C. Pollak, A. Rosa, E.J. Baerends, J. Am. Chem. Soc. 119 (1997) 7324.
- [5] E.J. Baerends, A. Rosa, Coord. Chem. Rev. 177 (1998) 97.
- [6] A. Rosa, E.J. Baerends, S.J.A. van Gisbergen, E. van Lenthe, J.A. Groeneveld, J.G. Snijders, J. Am. Chem. Soc. 121 (1999) 10356.
- [7] K. Pierloot, E. Tsokos, L.G. Vanquickenborne, J. Phys. Chem. 100 (1996) 16545.
- [8] N. Ben Amor, S. Villaume, D. Maynau, C. Daniel, Chem. Phys. Lett. 421 (2006) 378.
- [9] N.A. Beach, H.B. Gray, J. Am. Chem. Soc. 90 (1968) 5713.
- [10] M. Kotzian, N. Rösch, H. Schröder, M.C. Zerner, J. Am. Chem. Soc. 111 (1989) 7687.
- [11] S.A. Trushin, W. Fuß, W.E. Schmid, K.L. Kompa, J. Phys. Chem. A 102 (1998) 4129.
- [12] S.A. Trushin, W. Fuß, W.E. Schmid, Chem. Phys. 259 (2000) 313.

- [13] S.A. Trushin, W. Fuß, K.L. Kompa, W.E. Schmid, *J. Phys. Chem. A* 104 (2000) 1997.
- [14] W. Fuß, W.E. Schmid, S.A. Trushin, *J. Phys. Chem. A* 105 (2001) 333.
- [15] W. Fuß, S.A. Trushin, W.E. Schmid, *Res. Chem. Intermed.* 27 (2001) 447.
- [16] V. Lehtovuori, P. Myllyperkiö, J. Linnanto, C. Manzoni, D. Polli, G. Cerullo, M. Haukka, J. Korppi-Tommola, *J. Phys. Chem. A* 109 (2005) 17538.
- [17] J.K. Burdett, J.M. Grzybowski, R.N. Perutz, M. Poliakoff, J.J. Turner, R.F. Turner, *Inorg. Chem.* 17 (1978) 147.
- [18] C. Daniel, A. Veillard, *Nouv. J. Chim./New J. Chem.* 10 (1986) 83.
- [19] R.B. Jordan, *Reaction Mechanisms of Inorganic and Organometallic Systems*, Oxford Univ. Press, Oxford, 1991.
- [20] H. Ihee, J. Cao, A.H. Zewail, *Angew. Chem., Int. Ed.* 40 (2001) 1532.
- [21] M. Poliakoff, J.J. Turner, *Angew. Chem., Int. Ed.* 40 (2001) 2809.
- [22] M.J. Paterson, P.A. Hunt, M.A. Robb, O. Takahashi, *J. Phys. Chem. A* 106 (2002) 10494.
- [23] G. Worth, G. Welch, M.J. Paterson, *Mol. Phys.* 104 (2006) 1095.
- [24] S.A. Trushin, S. Panja, K. Kosma, W.E. Schmid, W. Fuß, *Appl. Phys. B* 80 (2005) 399.
- [25] S.A. Trushin, W. Fuß, K. Kosma, W.E. Schmid, *Appl. Phys. B* 85 (2006) 1.
- [26] S.A. Trushin, K. Kosma, W. Fuß, W.E. Schmid, *Opt. Lett.* 32 (2007) 2432.
- [27] W. Fuß, S. Panja, W.E. Schmid, S.A. Trushin, *Mol. Phys.* 104 (2006) 1133.
- [28] P. Hummel, J. Oxgaard, W.A. Goddard III, H.B. Gray, *Inorg. Chem.* 44 (2005) 2454.
- [29] webbook.nist.gov.
- [30] A.F. Schreiner, T.L. Broen, *J. Am. Chem. Soc.* 90 (1968) 3366.
- [31] Y.-J. Chen, C.-L. Liao, C.Y. Ng, *J. Chem. Phys.* 107 (1997) 4527.
- [32] S.A. Trushin, S. Sorgues, W. Fuß, W.E. Schmid, *ChemPhysChem* 5 (2004) 1389.
- [33] W. Fuß, W.E. Schmid, S.A. Trushin, *ISRAPS Bull.* 11 (2000) 7.
- [34] W. Fuß, W.E. Schmid, S.A. Trushin, *J. Chem. Phys.* 112 (2000) 8347.
- [35] V. Stert, H. Lippert, H.H. Ritze, W. Radloff, *Chem. Phys. Lett.* 388 (2004) 144.
- [36] U. Bastian, *Spektrum d. Wiss.* (February 2000) 42. Available from <<http://astro.estec.esa.nl/SA-general/Projects/Hipparcos/hipparcos.html>>.
- [37] W. Fuß, T. Schikarski, W.E. Schmid, S. Trushin, K.L. Kompa, P. Hering, *J. Chem. Phys.* 106 (1997) 2205.
- [38] D.M. Rayner, Y. Ishikawa, C.E. Brown, P.A. Hackett, *J. Chem. Phys.* 94 (1991) 5471.
- [39] J.D. Simon, K.S. Peters, *Chem. Phys. Lett.* 98 (1983) 53.
- [40] L.J. Rothberg, N.J. Cooper, K. Peters, V. Vaida, *J. Am. Chem. Soc.* 104 (1982) 3536.
- [41] J.A. Welch, K.S. Peters, V. Vaida, *J. Phys. Chem.* 86 (1982) 1941.
- [42] V. Jonas, W. Thiel, *J. Chem. Phys.* 102 (1995) 8474.
- [43] A.B. Rocha, *J. Phys. Chem. A* 111 (2007) 4711.
- [44] N.J. Turro, *Modern Molecular Photochemistry*, Benjamin/Cummings, Menlo Park, 1991.
- [45] M. Kasha, *Disc. Faraday Soc.* 9 (1950) 14.
- [46] D. Adelman, D.P. Gerrity, *J. Phys. Chem.* 94 (1990) 4055.
- [47] S.-C. Yu, S.-B. Ko, J.B. Hopkins, *Bull. Korean Chem. Soc.* 16 (1995) 1043.
- [48] S.-B. Ko, S.-c. Yu, J.B. Hopkins, *Bull. Korean Chem. Soc.* 15 (1994) 762.
- [49] A.G. Joly, K.A. Nelson, *Chem. Phys.* 152 (1991) 69.
- [50] B.R. Johnson, C. Kittrell, P.B. Kelly, J.L. Kinsey, *J. Phys. Chem.* 100 (1996) 7743.
- [51] T.R. Fletcher, R.N. Rosenfeld, *J. Am. Chem. Soc.* 107 (1985) 2203.
- [52] J.P. Holland, R.N. Rosenfeld, *J. Chem. Phys.* 89 (1988) 7217.
- [53] J.P. Holland, R.N. Rosenfeld, *Chem. Phys. Lett.* 145 (1988) 481.
- [54] J. Kim, T.K. Kim, J. Kim, Y.S. Lee, H. Ihee, *J. Phys. Chem. A* 111 (2007) 4697.
- [55] A. Rosa, A.W. Ehlers, E.J. Baerends, G.J. Snijders, G. te Velde, *J. Phys. Chem.* 100 (1996) 5690.
- [56] J.J. Turner, J.K. Burdett, R.N. Perutz, M. Poliakoff, *Pure Appl. Chem.* 49 (1977) 271.
- [57] W. Fuß, W.E. Schmid, K.K. Pushpa, S.A. Trushin, T. Yatsuhashi, *Phys. Chem. Chem. Phys.* 9 (2007) 1151.
- [58] W.C. Troglor, S.E. Desjardin, E.I. Solomon, *Inorg. Chem.* 18 (1979) 2131.
- [59] M. Dantus, R.M. Bowman, M. Gruebele, A.H. Zewail, *J. Chem. Phys.* 91 (1989) 7437.
- [60] M. Gruebele, G. Roberts, A.H. Zewail, *Phil. Trans. R. Soc. London A* 332 (1990) 223.
- [61] C. Daniel, J. Full, L. González, C. Lupulescu, J. Manz, A. Merli, S. Vajda, L. Wöste, *Science* 299 (2003) 536.
- [62] C. Daniel, J. Full, L. González, C. Kaposta, M. Krenz, C. Lupulescu, J. Manz, S. Minemoto, M. Oppel, P. Rosendo-Francisco, S. Vajda, L. Wöste, *Chem. Phys.* 267 (2001) 247.
- [63] S.A. Trushin, T. Yatsuhashi, W. Fuß, W.E. Schmid, *Chem. Phys. Lett.* 376 (2003) 282.
- [64] T. Yatsuhashi, S.A. Trushin, W. Fuß, W. Rettig, W.E. Schmid, S. Zilberg, *Chem. Phys.* 296 (2004) 1.
- [65] W. Fuß, W. Rettig, W.E. Schmid, S.A. Trushin, T. Yatsuhashi, *Farad. Disc.* 127 (2004) 23.
- [66] S. Sorgues, J.M. Mestdag, J.P. Visticot, B. Soep, *Phys. Rev. Lett.* 91 (2003) 103001.
- [67] M. Bixon, J. Jortner, *J. Chem. Phys.* 107 (1997) 1470.
- [68] J. Nasielski, A. Colas, *Inorg. Chem.* 17 (1978) 237.
- [69] W. Fuß, S. Lochbrunner, A.M. Müller, T. Schikarski, W.E. Schmid, S.A. Trushin, *Chem. Phys.* 232 (1998) 161.
- [70] W. Fuß, W.E. Schmid, S.A. Trushin, *Chem. Phys.* 316 (2005) 225.
- [71] G.G. Balint-Kurti, D.G. Truhlar, T.J. Martínez, N. Gidopoulos, C.H. Greene, A. Brown, D.R. Yarkony, H. Köppel, M. Collins, G.A. Arteca, V. Sundström, W. Fuß, V. Blanchet, M.S. Child, I. Burghardt, B. Kohler, W. Buma, B. Soep, J.C. Tully, C. Woywod, C. Evenhuis, O. Tapia, C. Zhu, E. Baloitca, et al., *Farad. Disc.* 127 (2004) 81.
- [72] M. Dzvonik, S. Yang, R. Behrson, *J. Chem. Phys.* 61 (1974) 4408.
- [73] D. Imre, J.L. Kinsey, A. Sinha, J. Krenos, *J. Phys. Chem.* 88 (1984) 3956.
- [74] T. Shimanoichi, *Tables of molecular frequencies consolidated*, NSRDS-NBS 39, 1972.
- [75] G. Herzberg, *Spectra of Diatomic Molecules*, Molecular Spectra and Molecular Structure, Van Nostrand Reinhold, New York, 1950.